Mafic pyroclastic flows at Santa Maria (Gaua) Volcano, Vanuatu: the caldera formation problem in mainly mafic island arc volcanoes

Claude Robin[1], Jean-Philippe Eissen[2] and Michel Monzier[1]
[1]ORSTOM, UR 14, A. P. 1711 06596 CCI Quito, Ecuador; [2]ORSTOM, UR 14, B.P. 70, 29280 Plouzané, France.

ABSTRACT

At Santa Maria Volcano (New Hebrides island arc), extensive ash and scoria flow deposits overlie the mainly effusive, pre-caldera cone. Hydromagmatic features characterize these deposits, the composition of juvenile clasts ranges from basalt to acid andesite/dacite (SiO_2 = 51–63.6%) with a dominant basaltic composition. The stratigraphic position of this pyroclastic series and its spatial distribution around a 8.5 km × 6 km wide caldera provide evidence of a relationship between this series and the caldera formation. In addition, these pyroclastic deposits are co-genetic to parasitic cones and lava flows developed along faults concentric to the caldera. Both series result from a compositionally layered magma reservoir, the subordinate differentiated magmas being the result of fractional crystallization from the basalts. A model of caldera formation which implies a large hydromagmatic eruption at the central vent and minor magma withdrawal by flank eruptions is proposed. This model emphasizes the importance of mafic hydroclastic eruptions in the caldera forming event and contradicts a model implying only quiet subsidence, a process often proposed for the formation of calderas in island arc volcanoes of mainly mafic composition.

Terra Nova, **7**, 436–443, 1995.

SUMMARIZED STRUCTURE OF SANTA MARIA VOLCANO AND OBJECTIVES

Basaltic pyroclastic flows are generally related to hydromagmatic processes and are generated by explosive eruptions which involve small volumes of magma, such as those from maars. Voluminous basaltic or mafic pyroclastic flows are extremely rare (e.g. Masaya in Nicaragua–Williams 1983: Bice 1985; Ambrym and Tanna in Vanuatu–Robin *et al.* 1993, 1994). Except for these few examples, mafic pyroclastic flows are not considered to play any role in caldera forming events, which are in some cases associated with andesitic pyroclastic flows (e.g. Cosiguina, Tambora), or more frequently with the emission of large volumes of evolved, felsic material. Moreover, most calderas on mainly effusive, poorly differentiated volcanoes, appear to be formed by quiet subsidence, following flank emission of lava flows.

In the northern Vanuatu Arc, Santa Maria island (also named Gaua; 167°30'E; 14°15'S; 330 km^2) corresponds to the emerged part of a 3000 m-high and 40 km-wide composite volcano. The island consists of a little-dissected symmetrical cone, about 25 km-across, truncated at an elevation between 500 m and 690 m by a 8.5 km × 6 km central caldera, and transected by faults in two main directions (60° and 320°; Fig. 1). The caldera hosts an active cone (Mt Garet, about 350 m high; base 3 km in diameter) which is bounded by a crescent-shaped lake.

Previous study of the geology has been presented by Mallick and Ash (1975): over the remnants of an ancient edifice, volcanics from the main cone appear to be wholly subaerial and are represented by a thick pile of basaltic and andesitic lava flows with associated rubble horizons and beds of red cinders or agglomerates. Mallick and Ash also recognized an extensive cap of ash surrounding the caldera. On the flanks, small parasitic cones and fissure-fed lava flows are distributed along fractures concentric to the caldera rim. The morphology of vents and lava surfaces mantling the lower slopes suggest that these peripheral extrusions are very young.

In this context, the caldera was believed to have been formed by quiet collapse of the central part of the main cone. On the lower slopes, an extensive series of mafic ash and scoria flows, not reported by previous workers, has been identified and sampled during recent fieldwork. These pyroclastic deposits allow us to reconsider the caldera formation in terms of explosive dynamics. In the following sections, we briefly describe these deposits and compare their petrology to that of the peripheral lava flows in order to propose a model for caldera formation with implications for the structure of the shallow magmatic system.

THE SANTA MARIA PYROCLASTIC SERIES (SMPS)

Stratigraphic sections from this series (location Fig. 1) are presented in detail by Robin *et al.* (1993). Along the southern coast, cliffs expose a composite sequence of both non-reworked and

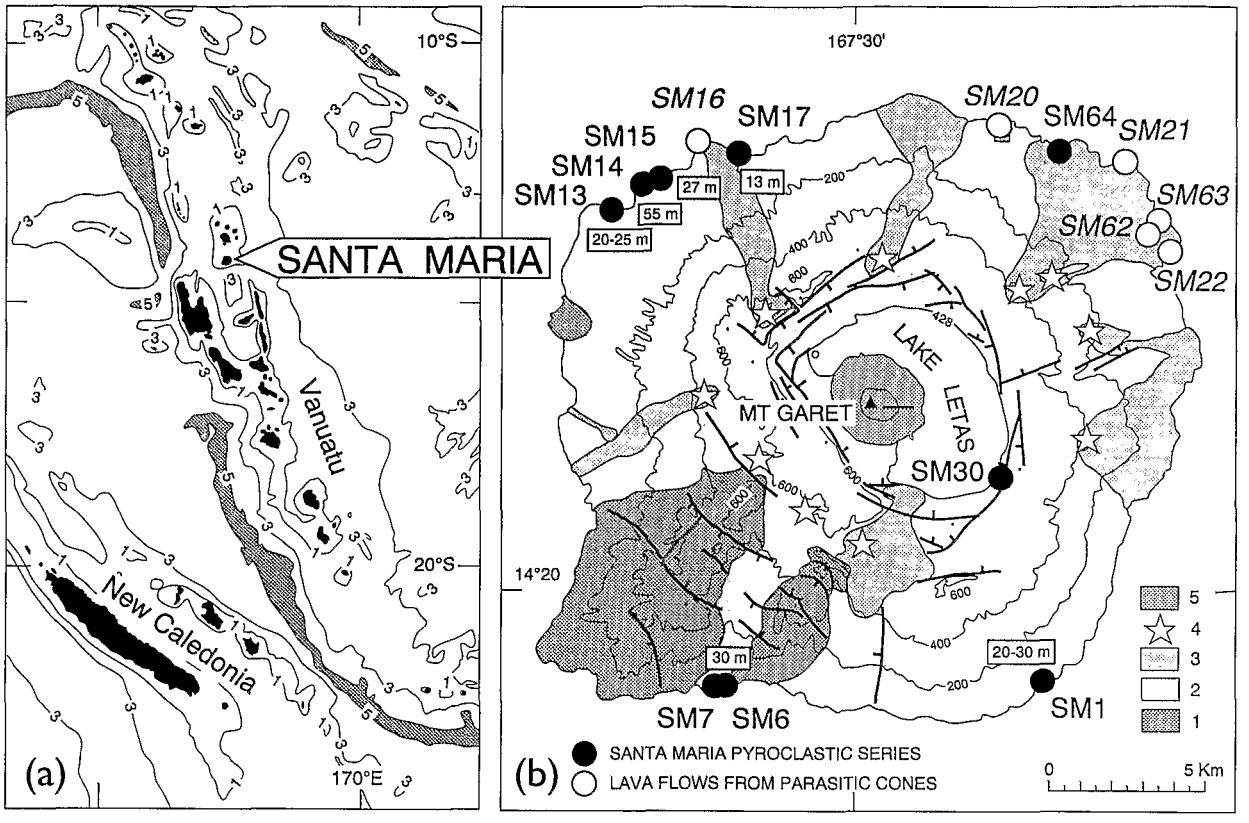

Fig. 1. *(a) location of Santa Maria in the central part of the New Hebrides Arc. Dotted area: New Hebrides Trench. Bathymetry in kilometers. (b) Geological sketch map of Santa Maria island, after Mallick and Ash (1975) modified, showing the location of studied outcrops of the SMPS. Thickness of the pyroclastic sequences are reported beside each site number. 1, old edifice; 2, main cone (essentially SMPS deposits overlying the basal edifice); 3, external lava flows; 4, Parasitic cones; 5, Active Mount Garet volcano.*

slightly reworked pyroclastic deposits which overlie the volcanics of the pre-caldera edifice. At sites 1, 6 and 7, a 20–30 m thick sequence consists of massive unsorted and indurated ash flows, including up to 50% by volume of coarse juvenile clasts: quenched lapilli with a very wide range of vesicularity from dominant dense angular blocks of glass to cauliflower bombs and subordinate pumice. Accidental clasts form 5–10% of the volume of the upper deposits, but in the 15 m-thick lower unit, at sites 6 and 7, there are 30–40% of accidental blocks. No buried soil has been observed between the successive flow units, which were probably emplaced in a short time interval.

In the north, over 6 km of continuous outcrop (sites 13–17, Fig. 1), at least three thick indurated pyroclastic flows are interbedded with fallout tephra and thinner beds of pyroclastic flows, and overlain by thick fall deposits, forming a complex sequence of about 60 m total thickness. This sequence enters the sea and its lower part could not be observed. Common facies of the ash flow deposits are massive to diffusely layered beds, 5–8 m thick, showing incipient bedding defined by alternating fine and coarse ash which includes glass lapilli, dense scoria bombs, pumice and lithic fragments. Between the massive units, surge deposits develop. In contrast to the southern examples, these deposits contain scarce accidental clasts (less than 5% in Vol.). The upper well-bedded ashfall layers contain accretionary lapilli beds and alternate with additional ash flow deposits and surges; these latter being 6 m-thick at site 15. A remarkable 3–4 m-thick andesitic pumice fall layer (sample SM 17E, Table 1) forms the upper deposit observed along the northern coast.

Due to the dense vegetation, deep soil and lack of access, continuous outcrops could not be observed over the cone. A section is provided by the Lusal River which carves into the east flank from the seashore up to the caldera rim. This section confirms that the cone consists mainly of lava flows. Nevertheless, this lava pile is covered by 30–40 m of yellow-brown weathered ashes bearing millimeter-sized dense vitric clasts. These ash deposits, previously reported by Mallick and Ash (1975), cover a nearly circular area, 7–8 km in radius from the centre of the volcano. Along the eastern lakeside, the ash deposits grade into stratified tuffs which show a 10° dip towards the centre of the caldera. Since these tuffs (SM 30 A, Table 1) have a geochemistry drastically different from the monotonous low-K basalt series from Mt Garet (see for comparison the average of 16 analyses from Garet, Table 1), the possibility of a relationship with the post-caldera volcanism is ruled out and

Table 1. (a) Whole-rock analyses (major and trace elements) of juvenile clasts from the SMPS and external lava flows. For comparison, the average and standard deviation of 16 analyses of basalts from Mount Garet is reported. Analyst: J. Cotten, Universite de Bretagne Occidentale and GDR-GEDO, Brest (France). (b) Averages of glass compositions calculated following the peaks at 52–53%, 56–57% and 62% SiO_2 observed on Fig. 2.

a

	SMPS (whole-rocks)														*External lava flows from parasitic cones (whole-rocks)*						*GARET*
Sample n°	SM 7A	SM 13C	SM 13A	SM 13B	SM 14B	SM 1C	SM 13D	SM 14A	SM 17E	SM 6C	SM 17D	SM 30A	SM 64A	SM 64B	SM 20	SM 62	SM 16	SM 63	SM 21	SM 22	Av. (16)
SiO2 (wt%)	51.50	51.60	51.70	52.00	52.00	55.15	55.30	55.60	56.70	57.20	57.50	58.00	63.60	63.60	53.50	54.70	55.40	56.60	56.70	57.00	50.57
TiO2	0.89	0.85	0.86	0.87	0.85	0.86	0.70	0.87	0.86	0.88	0.83	0.74	0.49	0.49	0.81	0.80	0.83	0.78	0.76	0.76	0.79
Al2O3	17.20	16.80	16.97	16.95	16.58	16.20	16.40	16.60	17.00	16.34	16.32	16.75	16.80	16.85	16.75	17.80	17.60	17.18	17.50	17.16	18.34
Fe2O3*	11.50	10.82	10.94	11.05	10.94	9.65	7.75	9.65	8.52	8.20	8.00	8.00	4.01	4.07	10.35	8.80	9.21	8.16	8.30	8.25	10.91
MnO	0.24	0.22	0.23	0.23	0.23	0.24	0.22	0.24	0.24	0.23	0.23	0.20	0.15	0.15	0.23	0.20	0.23	0.21	0.21	0.20	0.22
MgO	3.90	3.76	3.95	3.95	3.84	2.68	1.95	2.76	1.84	1.89	1.61	2.25	0.64	0.64	3.84	2.73	2.46	2.38	2.48	2.43	4.44
CaO	8.40	8.02	8.25	8.39	8.15	6.00	4.10	6.05	4.13	4.95	3.88	5.22	1.60	1.62	8.20	6.40	6.37	5.33	5.75	5.25	10.55
Na2O	3.28	3.99	3.54	3.61	3.35	4.27	4.30	4.34	4.12	4.82	4.56	4.60	5.62	5.62	3.83	4.20	4.43	4.62	4.62	4.52	2.82
K2O	1.80	2.25	2.17	2.16	1.89	3.00	3.46	3.07	3.21	4.06	3.61	3.40	5.35	5.74	2.60	3.06	3.31	3.62	3.21	3.41	1.01
P2O5	0.38	0.40	0.41	0.42	0.37	0.52	0.37	0.55	0.52	0.69	0.52	0.40	0.16	0.15	0.40	0.41	0.55	0.41	0.40	0.40	0.18
LOI 1050°C	1.45	1.37	0.88	0.47	2.33	1.26	5.28	0.87	3.02	1.04	3.13	0.41	0.53	0.52	0.07	0.56	0.05	-0.06	0.28	0.53	0.25
Total	100.54	100.08	99.90	100.10	100.53	99.83	99.83	100.60	100.16	100.30	100.19	99.97	98.95	99.45	100.58	99.66	100.44	99.23	100.21	99.91	100.07
Sc (ppm)	20.0	19.5	20.0	20.0	20.0	14.0	11.5	14.0	10.0	11.5	10.0	11.0	4.8	5.0	20.0	14.2	12.5	11.8	12.0	12.0	24.6
V	330	335	322	330	319	240	137	250	156	180	140	200	27	28	290	270	247	215	220	220	444
Cr	3	3	10	4	3	1	10	2	2	2	3	2	3	3	20	5	2	3	3	2	6
Co	32	30	30	31	30	24	17	24	17	18	13	17	5	4	29	23	23	19	19	19	33
Ni	8	12	12	10	12	2	7	4	2	1	2	4	1	2	14	8	5	2	3	3	11
Rb	29	38	38	38	33	54	66	53	62	71	69	62	108	110	36	46	54	60	43	59	14
Sr	800	820	820	825	805	745	580	770	680	650	624	680	210	211	810	765	925	685	710	660	935
Y	28	26	25	25	24	30	32	31	35	38	35	27	31	32	26	26	31	27	28	27	18
Zr	95	92	90	92	91	120	150	125	148	161	159	135	225	224	106	115	126	135	133	132	47
Nb	2.40	2.05	2.35	2.50	2.20	3.00	3.75	2.95	2.95	3.65	3.70	3.20	4.95	4.85	2.15	3.45	2.95	3.00	3.55	3.10	1.43
Ba	550	558	543	532	510	705	760	730	855	880	928	855	1050	1060	650	765	795	875	885	844	352
La	20.00	21.00	19.40	19.25	16.90	25.45	28.00	25.00	30.00	33.50	31.50	25.00	39.50	62.00	21.50	23.00	28.00	24.00	24.50	24.25	8.85
Nd	27.00	27.00	25.00	25.00	23.00	32.00	33.00	33.00	36.00	42.00	39.00	29.00	33.00	48.00	26.00	28.00	32.00	29.00	29.00	29.00	13.53
Eu	1.80	1.70	1.60	1.65	1.60	1.95	1.75	1.90	1.95	2.25	1.95	1.70	1.30	1.30	1.60	1.65	1.90	1.70	1.70	1.75	1.21
Dy	4.50	4.60	4.40	4.20	3.90	5.20	5.30	5.00	5.60	6.10	5.60	4.60	4.70	5.10	4.50	4.60	4.90	4.60	4.60	4.60	3.16
Er	2.70	2.50	2.60	2.30	2.30	3.00	3.30	3.10	3.40	3.90	3.60	2.50	3.30	3.50	2.50	2.70	2.90	2.80	2.80	2.90	1.84
Yb	2.55	2.35	2.35	2.30	2.23	2.90	3.15	2.90	3.20	3.63	3.35	2.68	3.45	3.53	2.48	2.45	2.73	2.73	2.70	2.70	1.73

b

	SMPS glasses					
	Av. (99)	sd	Av. (55)	sd	Av. (6)	sd
SiO2	52.69	0.75	57.43	0.82	62.45	0.58
TiO2	0.86	0.15	0.94	0.24	0.58	0.01
Al2O3	16.17	1.37	15.69	1.80	16.50	0.21
FeO*	9.78	1.49	7.96	1.69	4.81	0.21
MnO	0.22	0.08	0.26	0.10	0.17	0.15
MgO	4.10	1.01	1.75	0.52	0.88	0.05
CaO	8.90	1.49	4.70	1.01	2.21	0.01
Na2O	3.71	0.58	4.81	0.40	5.24	1.76
K2O	2.01	0.63	4.25	0.72	5.30	0.24
P2O5	0.36	0.16	0.65	0.19	0.19	0.03
Total	98.80		98.44		98.33	

it is postulated that the whole cap of ash covering the main cone is chronologically equivalent to the coastal pyroclastic sequence.

Abundant obsidian blocks have been encountered up to 150 m in elevation in the river which reaches the NE coast at site 64 (Fig. 1). The precise origin of this important rock (the most differentiated of the volcano as a whole, see SM 64 Table 1) is unknown; nevertheless, its elevated location on the cone suggests that these blocks came from a glass-rich pyroclastic layer of the SMPS.

Average thicknesses of 30 m and 50 m have been considered for the pyroclastic flows which cover the flat SE and NW sectors, respectively, leading to an estimated volume of 1.4 km^3. Given an average thickness of 30 m for the ash fall deposits which mantle the upper part of the cone, their volume is ≈ 5.3 km^3. Thus, the volume of pyroclastic deposits on land is of the order of 6.5–7 km^3.

SUMMARIZED PETROLOGY OF THE SMPS

Most juvenile clasts from the SMPS are aphyric or poorly porphyritic (generally 2–3% phenocrysts; 6% maximum). Eleven bulk compositions are reported in Table 1. SiO_2 ranges from 51.5% to 58%. The composition of obsidian blocks from site SM 64 (63.6% SiO_2), is also reported in this Table.

In basalts, plagioclase ranges from An 88 to An 55 (mole%), whereas olivine ranges from Fo 75 to Fo 65. In basaltic andesites and andesites, plagioclase composition ranges from An 62 to An 40 and from An 56 to An 40, respectively, whereas olivine, which is Fo 70–59 in basaltic andesites, was not found in andesites. Despite a wide compositional range in the whole series, characterized by two peaks at An 55–60 and An 75–90 (Fig. 3), normal or reverse zoning in plagioclase is restricted to only 4–5% An. Olivine is rarely zoned (maximum difference between cores and rims of phenocrysts: 7% Fo in normal zoning). Pyroxene compositions show slight but significant evolution from basalts to andesites (En 44.5–42 in basalts vs. En 43–40 in andesites).

Two hundred and eighteen microprobe analyses of glass from 12 thin sections show SiO_2 contents ranging from 50% to 63%. Within a flow unit or several flow units from a sequence (e.g. samples from the lower part of sites 13–14, Fig. 2), or even within a single sample, glass composition may vary over a large range. In the upper pyroclastic flows of the sequence at sites 13–14, glass compositions are essentially basaltic (Fig. 2). The SiO_2 frequency histogram representative of the whole SMPS exhibits a main peak at 52–53% SiO_2 and two subordinate peaks at 56–57% and 62% SiO_2. Average compositions of these peaks are reported in Table 1. An additional peak at 64% SiO_2 on Fig. 2 corresponds to the obsidian blocks SM 64, which show no significant variations by microprobe analysis.

DISCUSSION

Hydromagmatism

The main part of the SMPS deposits have hydromagmatic characteristics, as

demonstrated by quenched juvenile clasts, cauliflower bombs, surge deposits, armoured lapilli, indurated or muddy matrix in the flow deposits, and accretionary lapilli beds. The absence of welded textures and fumarolic pipes also indicates rapid cooling and low temperatures during deposition. A few 'dry' fallout episodes produced ash and lapilli layers such as the upper pumice layer SM 17. By their constant size (less than 8 cm), obsidian blocks SM 64 represent chilled magma ejected with a pyroclastic flow rather than blocks derived from an eroded welded layer. As a whole, the SMPS corresponds to an eruption which was essentially hydromagmatic.

Petrological significance

Wide compositional variation across pyroclastic flow sequences or within a single pyroclastic flow have been already described (Lipman *et al.* 1966; Schminke 1976; Wright and Walker 1981; Gardeweg and Ramirez 1987). The reported compositions generally range from acid andesite or dacite to rhyolite, and are believed to represent the uppermost layers of large zoned magma chambers. Basaltic compositions in voluminous pyroclastic flows have only been reported in rare examples (Williams 1983; Freundt and Schmincke 1992; Robin *et al.* 1993). At Santa Maria, through the studied sequences, a compositional evolution is apparent within the stratigraphy: while lower deposits show a slightly greater andesitic composition, the overlying ash flows show a larger range in SiO_2, but are dominantly basaltic in composition (Fig. 2). Both the geochemical data such as the oxide vs. SiO_2 variations (Fig. 4) and the mineralogy of these rocks allow us to conclude that all the SMPS hydromagmatic and magmatic products resulted from partial emptying of a magma body having a compositional gradient from basalt to acid andesite/dacite imposed by crystal fractionation.

Relationships with the parasitic cones and external lava flows

The parasitic cones and Mount Garet show geochemical characteristics which are drastically different (Table 1, Fig. 4 and our work in progress on Mount Garet). On the contrary, mineralogical comparison between the parasitic cones and the SMPS, summarized in Fig. 3 and in Table 2, suggests that the basalt and andesite lavas from the cones are co-genetic with the SMPS, a thesis corroborated by the whole-rock and trace-element geochemistry (Figs 4 and 5). The only differences between the centrally and laterally emitted rock

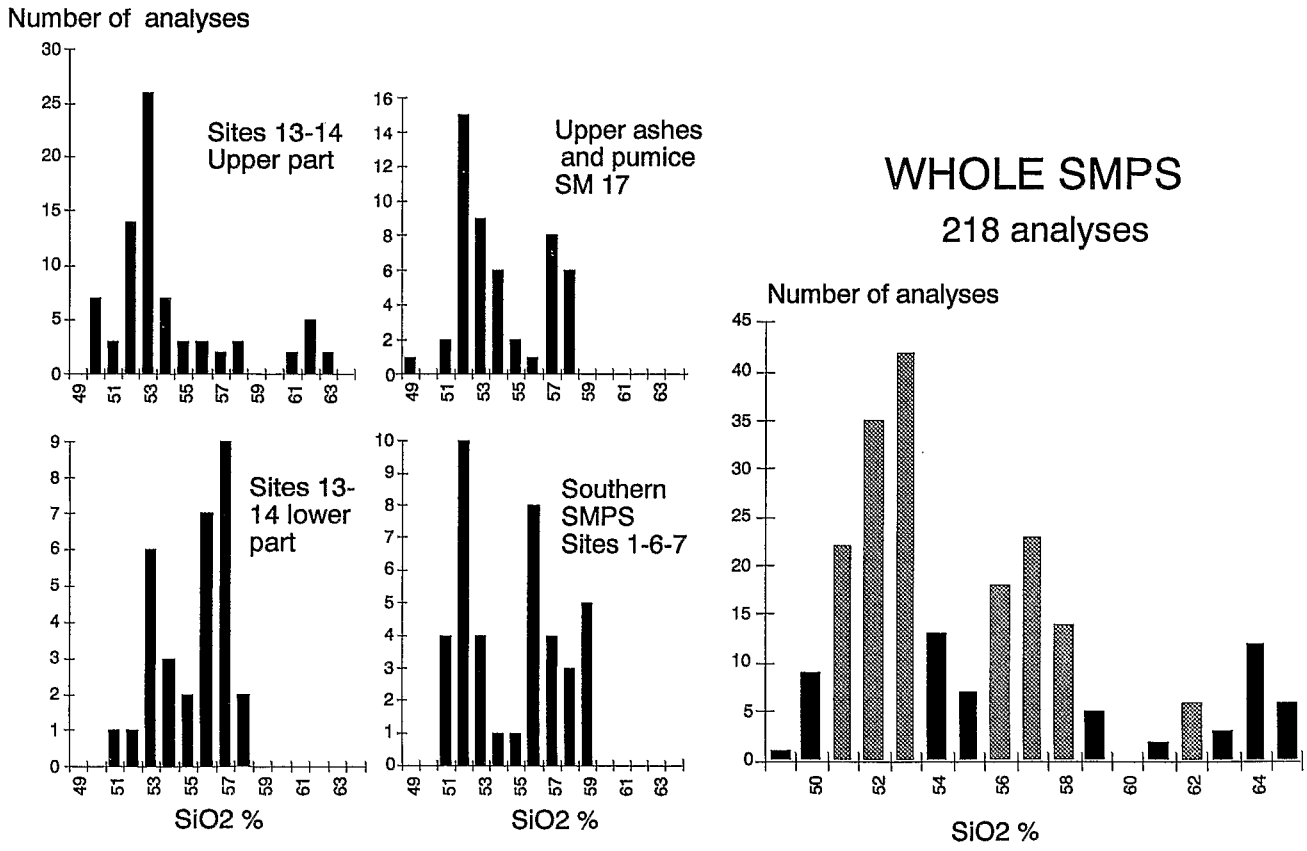

Fig. 2. *Frequency histograms for microprobe glass compositions in juvenile clasts from the SMPS. 'Class 55' = 55.00–55.99. Average compositions reported Table 1 are calculated for the stippled peaks. The peak at 64% SiO_2 on the whole SMPS histogram corresponds to microprobe analyses of obsidian bloks SM 64 (63.60% SiO_2, Table 1).*

series concern their phenocryst content and mineralogical zonings which are more developed in plagioclase and olivine from the cone series than in those from the SMPS (Fig. 3 and Table 2). This suggests a longer magmatic evolution for the magmas from the parasitic cones than for those erupted at the central vent.

Relationship with the caldera

On the north coast, the youthfulness of the flank extrusions is confirmed by the position of the lavas in lows, over the SMPS. If the possibility of a relationship between these lavas and the caldera formation exists, the role of the SMPS must also be considered. Several examples of basaltic or mafic pyroclastic flows of significant volume have been reported in volcanoes from the South West Pacific (Taylor 1956; Williams and Curtis 1964; Monzier *et al.* 1991; Robin *et al.* 1993, 1994). At Santa Maria, a relationship between the SMPS and the caldera-forming event is supported by the distribution of the pyroclastic deposits, and by their stratigraphic position at the top of the lava pile that is cut by the caldera scarp. Considering the relatively high density of the vitric tuffs, the DRE volume of the SMPS on land is 4–4.5 Km^3. This is enough to explain 35–40% of the volume of the caldera. To explain the entire volume, one has to consider: (i) that the greater part of the pyroclastic flows probably entered the sea (the volcano being about 3000 m high above sea bottom), and (ii) the possible participation of magma withdrawal by flank eruptions. In any case, the SMPS represents a large pyroclastic event which is at least in a large proportion responsible for the caldera collapse.

Model of caldera formation

A model of magma reservoir and caldera formation at Santa Maria volcano must take into account: (i) emission of an unknown volume of homogenous acid andesite/dacite (SM 64); (ii) large volumes of heterogenous (basaltic to andesitic) pyroclastic flows and fallout tephra related to a hydromagmatic phase, plus minor 'dry' andesitic tephra (layer SM 17E); (iii) co-genetic relationships of this pyroclastic series with the parasitic cones.

In major calderas associated with dacitic volcanoes, the potential for catastrophic vesiculation and volume increase due to pressure release at high levels in the chamber exists, making possible the violent eruption of a large volume of magma in a single plinian episode. Hydromagmatic explosions seem, on the face of it, confined to the interface between magma and water, and can therefore expel only a small proportion of magma (together with overlying roof rocks). Nevertheless, at Santa Maria, evidence for a single phase of mafic hydromagmatic eruptions, responsible for at least 35–40% of the depression, is clear. Although a plinian phase (samples SM 64) has probably occurred at the beginning of the event, the importance of the subsequent andesitic to basaltic hydromagmatism must be considered in the caldera formation. Since the caldera is a collapse structure and not an explosion (crater/maar) structure, it is proposed here that this structure resulted from a large hydromagmatic eruption followed by minor flank eruptions. The central eruption initiated with the ejection of differentiated products and was followed by

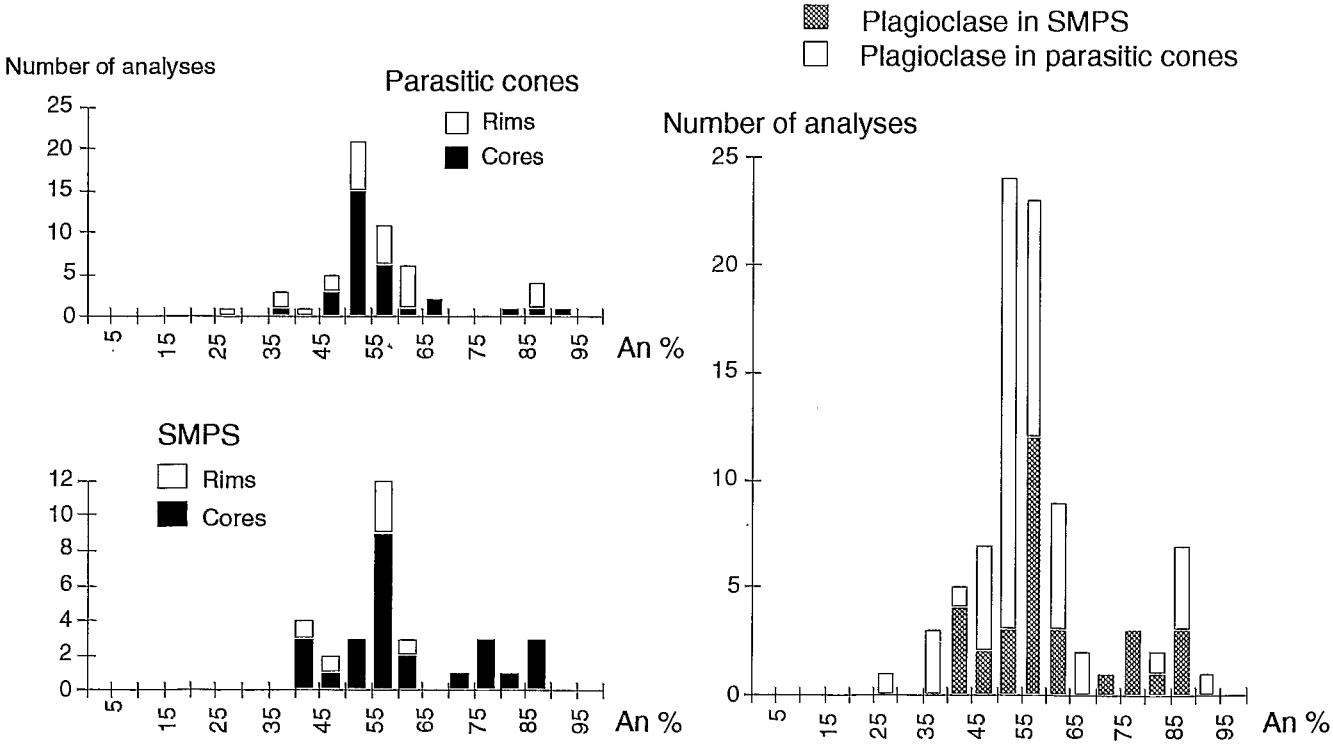

Fig. 3. *Frequency histogram for An content (mole%) in plagioclases in the SMPS and in lavas from parasitic cones.*

Table 2. Compared mineralogy between SMPS and lava flows from parasitic cones.

	SMPS juvenile clasts	Parasitic cones and fissure lava flows
Phenocrysts%	0–6%	8–22%
Plagioclase	An 40–87 Zoning: from −5 to +4% An (30 analyses)	Global range: An 29–90 Normal and reverse zonings from +11 to −23 An% Desequilibrium features (56 analyses)
Pyroxene	En 40–44; Fs 9–17 Not chemically zoned (28 analyses)	En 42–45; Fs 8–12 Not zoned (25 analyses)
Olivine	Fo 75–59 Rare normal zoning up to 7% Fo (14 analyses)	Compositions of cores: Fo 71–61 Global range: Fo 71–55 Reverse zonings up to 11% Fo (31 analyses)

produced overpressure at the top of this chamber, and massive overflow of hydrovolcanic products. Rapid convection induced by depressurization below the vent was responsible for the heterogeneous (basalt/andesite) 'mixed' magma recognized in the SMPS. As water penetration and vesiculation extended downward in the conduit, the mainly basaltic magma (upper pyroclastic flows) erupted, allowing caldera collapse. The origin of the acid andesite fraction shown in Fig. 2 (top left) is interpreted as a minor residual magma from the differentiated layer in the chamber. Due to the rapidity of eruption, no trace of mixing or equilibration between the different compositions is observed in the resulting products. Although the relative volumes of the evolved and mafic magmas cannot be constrained, the present data argue in favour of a shallow, mainly mafic reservoir.

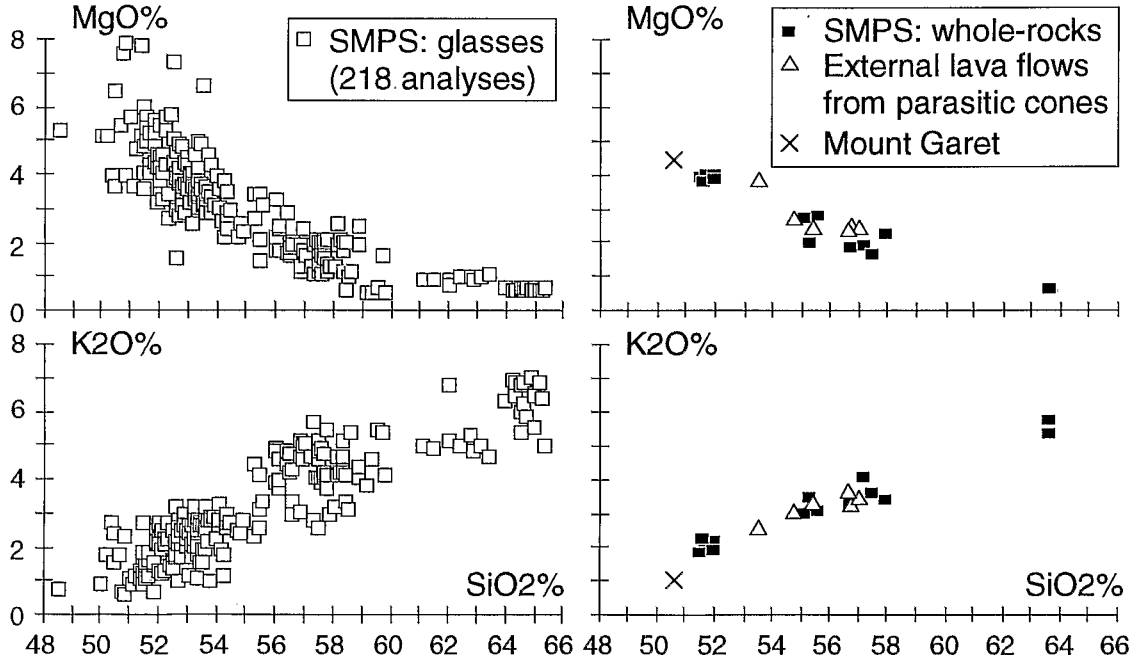

Fig. 4. *MgO and K_2O vs. SiO_2 diagrams for glasses analysed by microprobe in the SMPS and for the whole-rock analyses from the SMPS and peripheral lava flows from parasitic cones. For comparison, the average composition of 16 analyses from Mount Garet is also reported (X).*

mafic ones. As for andesitic eruptions leading to caldera collapse (Coseguina: Self *et al.* 1989; Tambora: Sigurdsson and Carey 1989), the intervention of externally derived water is required to force evacuation of large volumes of mafic magma. The summit of the pre-caldera cone was probably occupied by a large crater or a previous caldera (of the hawaiian type?) with a lake. Such a disposition is presently observed in Aoba volcano, 110 km to the south, at the southern end of the Aoba Basin. At this stage, the boundary of the present caldera was probably defined by circumferential eruptive fissures in a pattern comparable to that observed in the Galapagos type (Chadwick and Howard 1991). After a period of quiescence leading to the differentiation of magmas and moderate compositional zoning in the shallow chamber, gas pressure in the high-level reservoir increased, but probably not sufficiently to produce the eruption. Introduction of water into the upper magmatic column

The central explosive event may have been accompanied–or even preceded–by lateral emission of lava flows, but the bulk of the peripheral extrusions occurred after the cataclysm. Thus, it is suggested that the parasitic cones are related to *lateral* remnant apophyses of the reservoir. When the central eruption

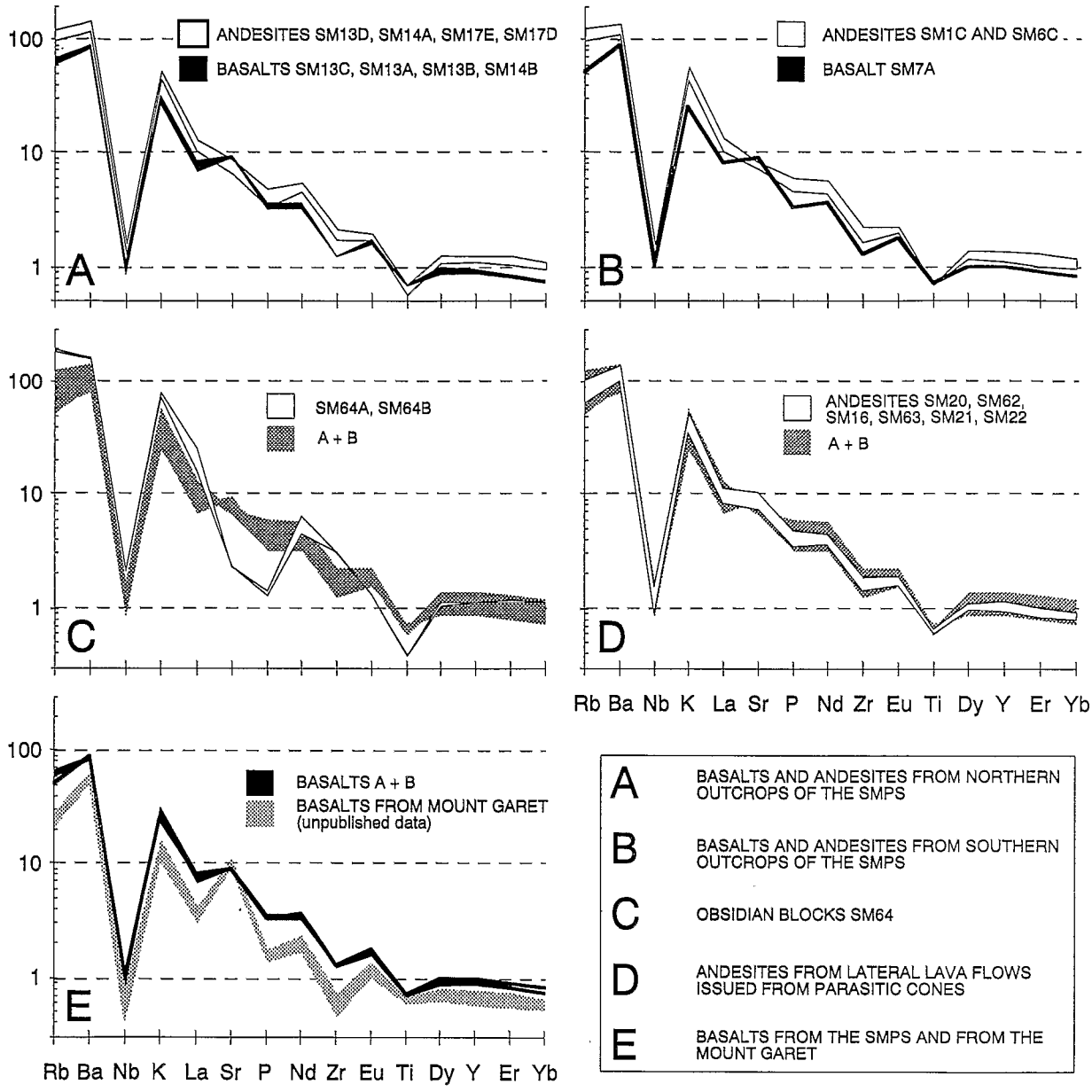

Fig. 5. *N-MORB normalized spidergrams for juvenile clasts from the SMPS and samples from peripheral lava flows and Mount Garet.*

occurred, the crystallizing magma in these lateral apophyses experienced convection, induced by general depressurization in the reservoir and/or by the ascending basalt below the central vent. The mineralogic zoning observed in the peripheral lavas give evidence of a new equilibrium between minerals and liquid before eruption.

Such a model may be compared to the caldera formation at Ambrym (Robin *et al.* 1993), another mainly basaltic volcano from the central New Hebrides arc, although at Ambrym typical maar deposits form a large tuff cone around the caldera (Monzier *et al.* 1991) and there is evidence for progressive enlargement of the caldera. In any case, at Santa Maria, like at Ambrym, field evidence underlines the role of hydrobasaltic eruptions in caldera formation, and contradicts a model implying only quiet subsidence due to magma withdrawal by flank eruptions, a common process proposed for the formation of calderas in volcanoes of mainly mafic composition.

ACKNOWLEDGEMENTS

This work is part of a research program developed at the Department of Geology, Mines and Water Resources in Vanuatu. It was financially supported by ORSTOM UR 14 and French Foreign Affairs Ministry (MAE). We thank S. Temakon, Director of the Department of Geology, Mines and Water Resources of Vanuatu, D. Charley for his help during the field work and *RV Alis's* captain Le Boulch and his crew. The authors are

also indebted to Dr M. Hall, Dr K-A. Erhenberg and an anonymous reviewer for constructive and helpful comments of the manuscript. Marcel Bohn and Joseph Cotten are deeply thanked for their help in performing the geochemical analyses.

REFERENCES

Bice D.C. (1985) Quaternary volcanic stratigraphy of Managua, Nicaragua: correlation and source assignment for multiple overlapping plinian deposits, *Bull. geol. Soc. Am.*, **96**, 553–566.

Chadwick W.W. and Howard K.A. (1991) The pattern of circumferential and radial eruptive fissures on the volcanoes of Fernandina and Isabela islands, Galapagos, *Bull. Volcanol.*, **53**, 259–275.

Freundt A. and Schmincke H-U. (1992) Mixing of rhyolite, trachyte and basalt magma erupted from a vertically and laterally zoned reservoir: composite flow P1, Gran Canaria, *Contr. Min. Petrol.*, **112**, 1–19.

Gardeweg M. and Ramirez C.F. (1987) La Pacana caldera and the Atana Ignimbrite. A major ash-flow and resurgent complex in the Andes of northern Chile, *Bull. Volcanol.*, **49**, 547–566.

Lipman P.V. and Christiansen R.L. (1964) Zonal features of an ash-flow sheet in the Piapi Canyon Formation. Southern Nevada, *Prof. Pap. US Geol. Surv.*, **501-B**, 74–78.

Lipman P.W., Christiansen R.L. and O'Connor J.T. (1966) A compositionally zoned ash-flow sheet in southern Nevada, *Prof. Pap. US Geol. Surv.*, **524-F**, 1–47.

Mallick D.I.J. and Ash R.P. (1975) *Geology of the Southern Banks Islands.* New Hebrides Geological Survey Reports, 33 pp.

Monzier M., Robin C., Eissen J-P. and Picard C. (1991) Découverte d'un large anneau de tufs basaltiques associé à la formation de la caldéra d'Ambrym (Vanuatu, SW Pacifique), *C. R. Acad. Sci. Paris*, **2**, 312, 1319–1326.

Robin C., Eissen J-P. and Monzier M. (1993) Giant tuff cone and 12 km-wide associated caldera at Ambrym volcano, New Hebrides Arc, *J. Volcanol. Geotherm. Res.*, **55**, 225–238.

Robin C., Monzier M., Crawford A. and Eggins S. (1993) Volcanology, petrology, geochemistry and tectonic evolution of the New Hebrides island arc. General Assembly, IAVCEI conference, Canberra, Sept 1993, Excursion guide A5, 86 p.

Robin C., Eissen J-P., Monzier M. (1994) Ignimbrites of basaltic andesite and andesite compositions from Tanna, New Hebrides Arc, *Bull. Volcanol.*, **56**, 10–22.

Schminke H.U. (1976) Geology of the Canary islands. In: *Biogeography and Ecology in the Canary islands* (ed. by G. Kunkel), pp. 67–184. W. Junk, The Hague.

Self S., Rampino M.R. and Carr M.J. (1989) A reappraisal of the 1835 eruption of Cosiguina and its atmospheric impact, *Bull. Volcanol.*, **52**, 57–65.

Sigurdsson H. and Carey S. (1989) Plinian and co-ignimbrite tephra fall from the 1815 eruption of Tambora volcano, *Bull. Volcanol.*, **51**, 243–270.

Taylor G.A. (1956) Review of the volcanic activity in the Territory of Papua-New Guinea, the Solomon and New Hebrides islands, 1951–1953, *Bull. Volcanol.*, **18**, 25–37.

Williams C.E. and Curtis R. (1964) The eruption of Lopevi Volcano, New Hebrides, July 1960, *Bull. Volcanol.*, **27**, 423–433.

Williams S.N. (1983) Plinian airfall deposits of basaltic composition, *Geology*, **11**, 211–214.

Wright J.V. and Walker G.P.L. (1981) Eruption, transport and deposition of ignimbrite: a case study from Mexico, *J. Volcanol. Geotherm. Res.*, **9**, 111–131.

Received 18 April 1994; revision accepted 24 November 1994

APPENDIX

Geochemistry analytical techniques

Whole-rock analyses were performed at the Université de Bretagne Occidentale in Brest. Selected fragments were ground in agate. Powders were digested with a concentrated acid mixture (1:8 HNO_3-HF). Fluorides were then dissolved and HF neutralized with an H_3BO_3 solution. International standards (JB2, BEN, ACE, GSN, MICA-Fe) were used for calibration. Rb determination was performed by flame Atomic Emission Spectrometry. All other elements were determined by Inductively Coupled Plasma Emission Spectrometry. Relative standard deviation for major oxides: SiO_2 = 1%, TiO_2 = 3%, Al_2O_3 = 2%, Fe_2O_3 = 2%, MnO = 5%, MgO = 2%, CaO = 2%, Na_2O = 2%, K_2O = 3%, P_2O_5 = 4%. Limit of detection and relative standard deviation for trace elements: Rb = 1 ppm, 5%; Sr = 0.2 ppm, 5%; Sc = 0.25 ppm, 5%; V = 2 ppm, 5%; Cr = 1 ppm, 5%; Co = 1 ppm, 5–10%; Ni = 2 ppm, 5%; Zr = 1 ppm, 5%; Nb = 0.8 ppm, 5–10%; Y = 0.5 ppm, 5%; La = 0.8 ppm, 5%; Nd = 2 ppm, 10%; Eu = 0.2 ppm, 5–10%; Dy = 0.4 ppm, 5%; Er = 0.8 ppm, 10%; Yb = 0.2 ppm, 5%. Mineral and glass compositions were determined with the CAMECA SX50 automated microprobe at Brest), using mineral standards supplied by the BRGM (Orleans). Operating conditions: 15 KV accelerating potential, 10 mA beam intensity and 10 s count time.